Photocurable chitosan as bioink for cellularized therapies towards personalized scaffold architecture

Photocurable chitosan as bioink for cellularized therapies towards personalized scaffold architecture

*Chiara Tonda-Turo** [a,b], *Irene Carmagnola* [a,b], *Annalisa Chiappone* [b,c], *Zhaoxuan Feng* [d], *Gianluca Ciardelli* [a,b], *Minna Hakkarainen* [d], *Marco Sangermano* [b,c]

[a] Department of Mechanical and Aerospace Engineering, Politecnico di Torino, C.so Duca dgeli Abruzzi 24, 10129 Torino, Italy

[b] POLITO BIOMedLAB, Politecnico di Torino, Turin, Italy

[c] Department of Applied science and technology, Politecnico di Torino, C.so Duca degli Abruzzi 24, 10129, Torino, Italy.

[d] KTH Royal Institute of Technology, Department of Fibre and Polymer Technology, Teknikringen 56-58, 10044 Stockholm, Sweden

CORRESPONDING AUTHOR

* **Dr. Chiara Tonda-Turo**

Department of Mechanical and Aerospace Engineering, Politecnico di Torino, C.so Duca dgeli Abruzzi 24, 10129 Torino, Italy. chiara.tondaturo@polito.it

ABSTRACT

Recent progresses in tissue engineering are directed towards the development of technologies able to provide personalized scaffolds recreating the defect shape in a patient specific manner. To achieve this ambitious goal, 3D bioprinting can be combined with a suitable bioink, able to create a physiological milieu for cell growth. In this work, a novel chitosan-based hydrogel was developed combining photocrosslinking and thermo-sensitive properties. Commercial chitosan (CS) was first methacrylated and then mixed with β glycerol phosphate salt (β-GP) to impart a thermally induced phase transition. The absence of cytotoxic degradation products and the excellent biocompatibility of the developed hydrogel was confirmed through *in vitro* tests using different cell lines (NIH/3T3, Saos-2, SH-SY5Y). Cellularized 3D structures were obtained though 3D bioprinting technologies confirming the processability of the developed hydrogels and its unique biological properties.

KEYWORDS: chitosan, 3D bioprinting, bioinks, photocrosslinking, tissue engineering

INTRODUCTION

The new paradigm of tissue engineering and regenerative medicine (TERM) is grounded on personalized approaches to restore tissue defects by custom-made scaffolds that accurately reproduce the defect morphology and the complex organ structures.[1,2] Personalized custom-made scaffolds should allow to perfectly fit patient defects as well as mimic the complex geometry of tissues and organs.[3,4] The raise in new CAD/CAM technologies set up to process biomaterials and biological compounds have driven the replacement of injured tissues applying both biology and engineering principles.[5,6] For instance, modern rapid prototyping technologies have been applied to produce custom-made scaffolds to restore normal anatomy in bone defects,[1] maxillofacial defects,[7] skin grafts[8] as well as components of the human heart.[9] Furthermore, 3D printing technologies have found application in the development of organ-like platform for *in vitro* studies of diseases.[10] The implementation of 3D printing in the biomedical field has grown over the past few years and at the same time the number of novel biomaterial formulations to be processed through 3D printing has constantly increased. Successful printing can be achieved only by applying materials with high printability, printing fidelity and suitable mechanical properties. The implementation of bioprinting technologies that combine biomaterials, living cells and 3D printing technologies[3] to build cellularized scaffolds requires the development of cell-laden biomaterials able to simultaneously be printed, host cells in a proper environment, and accurately be deposited without causing cellular damages.[11] Despite its lower resolution compared to laser or inkjet-based cell printing technologies the micro-extrusion approach is widely employed for bioprinting as it is a simple and cost-effective method.[6] Micro-extrusion-based printers are composed of a bioink loaded syringe equipped with a mechanical actuator (screw or piston) which applies a physical force or a pressure on the syringe to dispense the bioink in controlled manner.[12] The printing head movement towards x,y,z axes is coordinated by a computer following a pre-defined architecture.

Several bioinks which fulfil printability requirements for micro-extrusion printing are currently available both for cell-laden and cell-free scaffold fabrication [13,14]. Among others, adjustable viscosity is a key feature as the bioink needs to be liquid in the syringe to avoid nozzle clogging and then it has to quickly become a hydrogel after deposition to maintain the 3D shape[12]. Phase changes during the printing process can occur in the bioink as a result of chemical or physical crosslinking inducing an increase of the viscosity as a function of crosslinking degree. Temperature or pH changes within the physiological range have been widely applied for this purpose.[15,16] However, the stability of the obtained hydrogels is often poor. Ionic crosslinking permits to achieve a higher stability in aqueous environment,[17,18,19] but it is limited to a restricted number of materials (e.g. alginate) and requires the continuous supply of ions in the aqueous environment to avoid dissolution. Photocrosslinking has emerged as a promising alternative since methacrylate-groups can be easily added to many biocompatible polymers without affecting their biocompatibility.[20] The presence of methacrylate groups enables the bioink to rapidly crosslink upon light irradiation (photocrosslinking) which enables printing of high resolution structures.[21,22]

To date, poly(ethylene glycol) diacrylate (PEGDA) and gelatin methacrylate (GelMa) are the most studied photocrosslinkable bioinks.[23],[24],[25],[26] Chitosan (CS) hydrogels are highly interesting materials for biomedical applications thanks to their generally good biocompatibility and excellent biological properties [27–29]. Several authors have proposed chitosan based solution blended with photocurable polymers (e.g. PEGDA) to impart photocrosslinkable features to bioartificial solutions [30,31]. However, recent protocols have reported the synthesis of methacrylated CS and its photocuring in aqueous solutions to produce hydrogels was also demonstrated [32,33]. Photocrosslinkable CS hydrogels have been applied as bioadhesives for soft and hard tissues,[34] transmucosal drug delivery systems,[35] scaffold for tissue regeneration[36] and cell-laden hydrogels for cell encapsulation.[37]. It is, therefore, of high interest to investigate the processability, curing properties and biocompatibility of photocrosslinkable CS as well as its potential as a bioink for cell encapsulation and 3D bioprinting of well-defined scaffold architectures. Here, we develop a novel

CS bioink with a dual crosslinking mechanism combining thermally induced gelation and photocrosslinking to enhance the stability and functional properties of the bioink. A dual crosslinking mechanism is a key requirement in bioprinting as the first crosslinking, mediated by temperature, guarantees the maintenance of the printed architecture while the second crosslinking, induced by UV irradiation, enhances the stability of the hydrogel in physiological environments. Commercial chitosan (CS) was methacrylated to enable dissolution in water and to impart photocrosslinking ability. The photocrosslinkable CS solution was further mixed with β glycerol phosphate salt (β-GP) to provide thermo-sensitive behaviour [38] and to adjust the pH around 7.4 to maximize the similarity with the physiological milieu. The photocuring properties, 3D bioprinting properties, cell viability and cell encapsulation ability of the CS based formulation were then examined.

EXPERIMENTAL SECTION

Synthesis and characterization of methacrylated CS

Methacrylated CS was prepared following the protocol reported by Feng et al[32]. Briefly, CS (medium molecular weight, Sigma-Aldrich) was dissolved at 1.5% w/v in acetic acid solution (2% w/v from glacial acetic acid, Sigma-Aldrich) at room temperature. Subsequently, CS solution temperature was set to 50°C, methacrylic anhydride (Sigma-Aldrich, 3.73 g) was slowly added and the reaction was carried out for 4 hours. The solution was then neutralized by adding 55.2 g of $NaCO_3$ 5 % w/w. The solution with methacrylated CS was dialyzed (Biotech Cellulose Ester Dialysis Membrane, MWCO = 1 kDa) in bi-distilled water for 4 days and then lyophilized. The methacrylation of chitosan was evaluated by ATR-FTIR. Infrared spectroscopy was performed using a PerkinElmer Spectrum 2000 FTIR spectrometer (Norwalk, CT) equipped with an attenuated total reflectance crystal accessory (Golden Gate). Spectra were obtained in the 4000 and 600 cm^{-1} wavenumber range at a resolution of 4 cm^{-1} and averaged over 32 scans. Spectra were analyzed by Spectrum software.

Preparation of photo and thermo crosslinked CS hydrogels

Methacrylated CS was dissolved in milli-Q water at a concentration of 1.5% w/v, stirred overnight and stored at 4°C. A β-glycerophosphate disodium salt hydrate (β-GP - Mw=306.123 g/mol, Santa Cruz Biotechnology) was prepared in culture medium (DMEM - Dulbecco's Modified Eagle Medium, Carlo Erba, Italy) by dissolving 500 mg of β-GP in 1 mL of media. Then, the β-GP solution was added drop-by-drop to 5ml of the methacrylated CS solution under continuous stirring in an ice-bath. Methacrylated CS/β-GP solution was stirred for 15 minutes and then 0.05% w/v of lithium phenyl-2,4,6-trimethylbenzoylphosphinate (LAP) was added as photoinitiator and stirred for 15 minutes. The final solution containing methacrylated CS, β-GP and LAP prior to temperature induced phase transition and UV irradiation was coded as ptCS solution. The pH of ptCS solution was 7.3± 0.1, measured using a pH meter (Hanna Instruments). All the described preparation steps were performed in a dark environment to protect the solutions from light. The ptCS solution was poured in petri dish and exposed to 37°C and UV light at 365 nm wavelength (Hamamatsu LC8 lamp emitting in the UV range, bulb type 365 nm, intensity 30 mW/cm^2) for 2 minutes to obtain a crosslinked hydrogel coded as ptCS hydrogel (figure 1). The thermo-sensitive behaviour of ptCS solution was qualitatively confirmed through tube inverting test which allows to determine the sol-gel transition rate[39] .

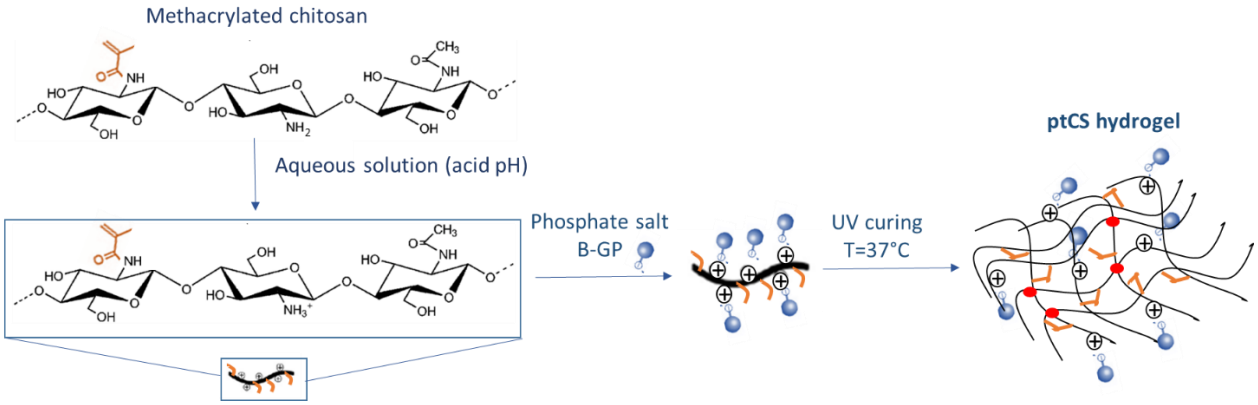

Figure 1. Scheme of the crosslinking hydrogel formation mechanism, red dots schematized the formation of hydrophobic interactions among CS chains [40,41].

Rheological tests

The thermo-sensitive behaviour as well as the photocrosslinking of the ptCS solution were monitored through rheological measurements using a stress-controlled rheometer (MCR302, AntonPaar GmbH, Graz, Austria) equipped with 25 mm parallel plate geometry. For each test, temperature was controlled with a Peltier system while de-hydration was prevented by a water trap.

A time sweep test was performed to measure the thermosensitive behaviour of ptCS solution applying a rotational oscillation at frequency of 1 Hz and a shear strain amplitude of 1%. The ptCS solution was poured on the refrigerated lower plate (0°C) and then the temperature was set at 37°C immediately after starting the test.

In order to evaluate the photocrosslinking kinetics, the instrument was set up with a bottom quartz plate and connected to a Hamamatsu LC8 lamp emitting in the UV range (bulb type 365 nm, maximum intensity 30 mW/cm^2) equipped with a flexible light guide. The gap between the two plates was set to 0.4 mm and the sample was kept at a constant temperature (37°C). Light was turned on after 1 min in order to stabilize the system. All the measurements were carried out in the linear viscoelastic region (strain amplitude 1%) and under rotational oscillation at frequency of 1Hz.

Quartz crystal microbalance with dissipation monitoring device (QCM-D) to monitor the crosslinking process

To further confirm the crosslinking mechanism of the ptCS solution, a quartz crystal microbalance with dissipation monitoring device (QCM-D -QSense Explorer) equipped with an open module was used to monitor changes in mass or viscosity after crosslinking. A Gold (Au) coated sensor (QSX301, Q-Sense, Sweden) was cleaned following manufacture's instruction prior to use and then 300 µL of ptCS solution was poured on the sensor. PtCS solution was heated at 37°C or exposed to UV light using a Hamamatsu LC8 lamp emitting in the UV range (bulb type 365 nm, maximum intensity 30 mW/cm^2) and odd overtones (3, 5, 7, 9, 11, 13) were monitored to evaluate changes in frequency (Δf) and energy dissipation factor (ΔD) at crystal fundamental resonance frequency (5 MHz).

Stability of ptCS hydrogel in aqueous environment

Stability tests were carried out on ptCS hydrogels. 1 mL of ptCS solution was poured into glass vials irradiated for 2 minutes and then immersed into 2 mL of culture medium that had been pre-warmed at 37°C. At defined time points (1 day, 3, 7, 14 and 28 days), culture medium was removed. The samples were weighted (W_{wet_i}), freeze-dried and weighted (W_{dry_i}) again. The weight loss (WL) were calculated as (1).

$$WL(\%) = \frac{W_{dryTeor} - W_{dry\_i}}{W_{dryTeor}} * 100 \quad (1)$$

where $W_{dryTeor}$ is the theoretically calculated weight of the dried sample at t=0. The changes in composition of ptCS hydrogel during the stability test was monitored through thermogravimetric analysis (TGA) using a TGA/DSC 1 Star System (METTLER TOLEDO) equipment. Samples were heated from 25°C to 600°C at a rate of 10°C/min in nitrogen atmosphere. After the different time points, the pH of the removed PBS was measured to confirm the maintenance of a physiological pH (7.2-7.4).

Assessment of ROS scavenging activity

The antioxidant properties of the ptCS hydrogel were assessed though an antioxidant assay (Total Antioxidant Capacity Assay Kit, MAK187 from Sigma), that measures the efficacy of antioxidant materials by quantifying the reduction of Cu^{2+} to Cu^{+}. The reduced Cu^{+} ions react with a colorimetric probe present in the assay solution and the absorbance peak of the probe is proportionally related to the antioxidant features of the tested material. 100 µL of ptCS solution was poured in each plate of a 24-well multiwall plate and exposed to UV light to induce photocrosslinking as previously described. Following the manufacturer's instructions, vitamin E analog (Trolox) solutions at different concentrations were used as a standard antioxidant to generate a calibration curve. Cu^{2+} working solution was added to the ptCS hydrogels and to the Trolox samples, incubated for 90 minutes at

room temperature and then, the absorbance was measured at 570 nm through a microplate reader (Victor3, PerkinElmer). All the values were corrected by subtracting the blank and the background (ptCS hydrogel soaked in water) and the experiment was repeated in triplicate. A CS-based hydrogel obtained using the same amount of non-methacrylated CS and β-GP was obtained and used as control.

CS-based solution as bioink for 3D bioprinting

Experiments on bioprinting of ptCS solution were done using a 3D bioprinter (Rokit Invivo 3D Bioprinter, RokitHealthcare). The bioprinter was equipped with a bio-dispenser to extrude bioinks in a temperature-controlled environment. Five mL of ptCS solution was loaded in a 12 mL plastic syringe and then placed in the printhead. Printhead temperature was set at 4°C while the printbed was heated at 37°C to induce the temperature-mediated phase transition of the ptCS solution. Before printing, calibration in the x and y axes was done automatically and calibration in the z axis was done manually. A multi-layer grid structure was realized using the NewCreatorK software (RokitHealthcare) and a 1 minute-stop was added between each layer to permit photopolymerization by manually turning on the UV-led (wavelength 365 nm) available below the printhead. Three tips were used having different diameters of 22G, 25G and 27G. The ptCS solution was printed on a Petri dish and then morphologically analyzed (Leica Z16 AP0A). Printed grids were frozen at -20°C for 24 hours and then freeze-dried (Scanvac, CoolSafe).

Cell viability assay: indirect tests

Cell viability assay was performed to evaluate the biocompatibility of the photocrosslinked hydrogels. NIH/3T3 cells (ATCC® CRL-1658™), Saos-2 (ATCC® HTB-85™) and SH-SY5Y (ATCC® CRL-2266™) were cultured on three different 96 multiwell plates at a cell density of 2×10^4 cells/well for 24 h to reach confluence using DMEM - Dulbecco's Modified Eagle Medium (Carlo Erba, Italy) for NIH/3T3 and SH-SY5Y, and McCoy's 5A Modified Medium (Thermo Fisher Scientific, Italy) for Saos-2. Simultaneously, ptCS hydrogels were soaked for 24 h in 1 mL of DMEM or McCoy's 5A

(Modified) Media each 0.1 g of ptCS hydrogel. After 24 h, media were collected and filtered through 0.22 µm filters to guarantee sterility.

Then, the culture medium was removed from each well of confluent cells and substituted with the supernatant collected from the ptCS hydrogels. Controls (CTRL) were obtained using normal medium. After 24 h incubation, the supernatant was carefully removed and the cell viability assay was performed using non-fluorescent resazurin, which is converted into a highly red fluorescent dye (resorufin) by cell metabolism. Briefly, a volume of 100 µL of 0.1 mg/mL resazurin solution was added in each well and the cultures incubated for 1 h at 37°C. The 0.1 mg/mL resazurin solution was obtained by diluting a resazurin working solution (1 mg/mL in phosphate buffered saline-PBS, Sigma Aldrich, Milan) into DMEM. Then, the fluorescent signal was monitored using a plate reader (Victor X3, Perkin Elmer) at 530 nm excitation wavelength and 590 nm emission wavelength. Cell viability was calculated as a percentage value compared to CTRL. Three samples for each condition were used and experiments were performed three times. GraphPad Prism® software was used for one or two way analysis of variance (ANOVA). Values * $p < 0.05$, ** $p < 0.01$, *** $p < 0.001$ were considered statistically significant.

Cell encapsulation and feasibility of cell loading bioprinting

NIH/3T3 cells were mixed to ptCS solution at a concentration of 100.000 cell/mL and then loaded into the syringe to be printed as previously described to preliminary evaluate the feasibility of the cell bioprinting and to qualitatively analyse the cell survival after processing. In order to prepare sterile ptCS solution the methacrylated CS powder was UV-sterilized for 15 min while the solutions were 0.22 µm-filtered prior to use.

PtCS solution mixed with cells was loaded into a 12 mL syringe stored into a 4°C printhead and then printed on 37°C-bed following two methods: 100 µL were poured to form drops or grid-shaped 1 layer structures. Immediately after printing, UV led was turned on for 1 minute to perform photocrosslinking. Live/dead staining (LIVE/DEAD®mcell Imaging Kit, Life Technologies, Thermo

Scientific, USA) was used to assess cell viability at 24, 48 and 120 h. Encapsulated cells were stained with 150 µL solution of 4 µM Ethidium homodimer-1 and 2 µM calcein in PBS and incubated for 40 minutes at room temperature. After staining, cells were imaged with a fluorescence microscope (Leica DMIL Led) to detect calcein (ex/em 488 nm/515 nm) and Ethidium homodimer-1 (ex/em 570 nm/602 nm), respectively.

RESULTS AND DISCUSSION

Chitosan was methacrylated with methacrylic anhydride to explore and exploit chitosan's good biocompatibility and excellent biological properties in photocurable bioinks for preparation of hydrogels for cellularized therapies.

Characterization of methacrylated CS

The successful of the methacrylation reaction was confirmed by infrared spectroscopy. ATR-FITR spectrum (figure 2) of CS powder and methacrylated CS (figure 2A,C) shows the characteristic absorption bands of chitosan[42] at 3300 cm^{-1} attributable to O-H and N-H stretching, at 1634 and 1548 cm^{-1} due to C=O stretching and N-H bending, respectively and at 1410 cm^{-1} due to C-N stretching. In addition, the FTIR spectrum showed the absorption bands diagnostic of methacrylic groups[32]**.** In particular, the peaks centered at 845 cm^{-1} and at 1617 cm^{-1} are characteristic of the C=C double bonds (figure 2C). The same analysis was repeated after UV-irradiation to monitor the success of the crosslinking reaction; the significant reduction of the C=C absorption bands intensity demonstrated the efficacy of the UV-curing process (figure 2B). Moreover, the absorption bands at 1052 and 961 cm^{-1} due to phosphate groups[43] revealed the presence of β-TCP in the photocured hydrogel (figure 2B).

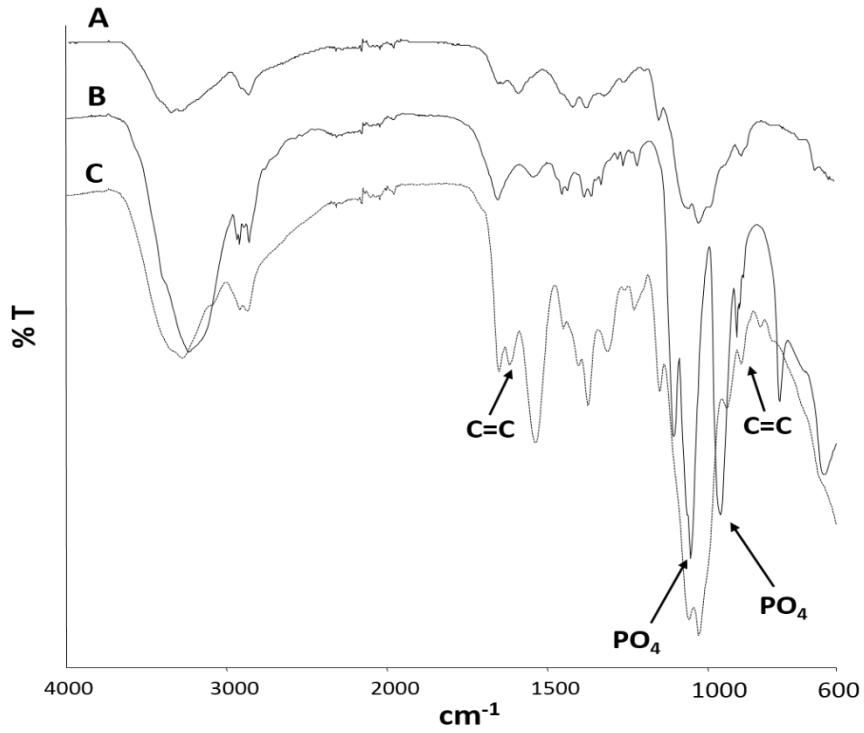

Figure 2. ATR-FTIR spectra of chitosan powder (A), freeze-dried ptCS hydrogel (B), methacrylated CS (C).

Rheological properties

Rheological measurements were performed to evaluate the thermosensitive behaviour of the ptCS as well as its reactivity towards photopolymerization. First of all, the thermosensitive behaviour of the ptCS solution was confirmed by time sweep test (figure 3A). The ptCS solution was poured on the rheometer plate at 0°C and the temperature was quickly increased up to 37°C. The G' and G'' modulus both increased reaching a plateau value after 40 seconds, confirming the effect of the temperature on the hydrogel mechanical properties.[15],[40] The subsequent photorheological study showed the high reactivity of the material with the fast increase of the G' modulus upon irradiation.[44,45]

Two different values of light intensity (3 and 30 mW/cm^2). were tested in order to simulate different curing conditions, taking into consideration that the UV LED apparatus set on the bioplotter reaches a rather low intensity The comparison of the two experiments result shows that the light dose has only a small influence on the curing kinetic of the polymer in the considered range (figure 3B). When the

intensity decreased (10% of the total intensity 3 mW/cm^2) the crosslinking rate decreased accordingly reaching a plateau in less than 40 sec. Furthermore, it can be observed that the final values of the elastic modulus G' (~6 kPa) obtained after 40 sec of irradiation, are in line with those reported in literature for other bio-printable 3D hydrogels, indicating the suitability of the proposed material for this kind of manufacturing technique[46].

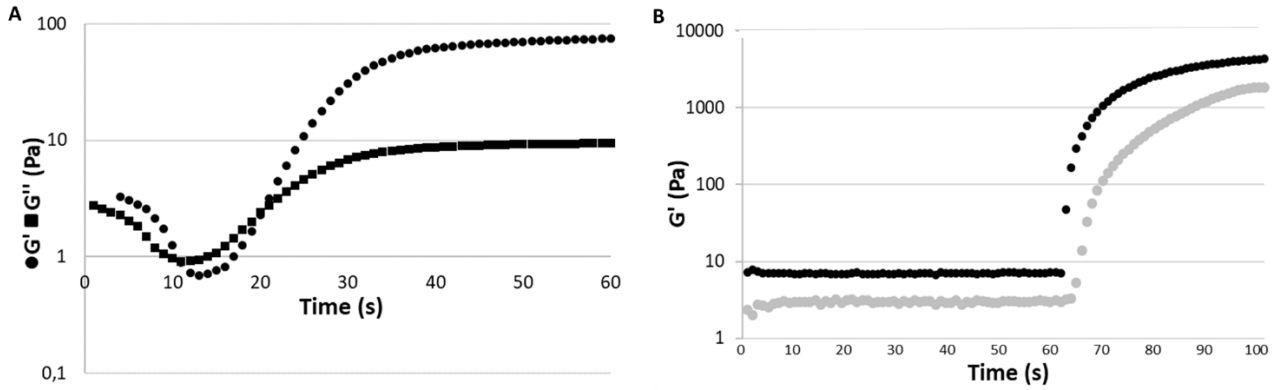

Figure 3. Time sweep tests on ptCS solution. A) time sweep test was performed to measure the thermo-sensitivity of the ptCS solution and G' and G'' were recorded increasing the temperature from 0° to 37°C immediately after test started. B) time sweep test was performed to evaluate the kinetics of the photocrosslinking using 10 % (grey) and 100 % (black) intensity. UV lamp at 365nm was turned on after 60 seconds.

Crosslinking process monitoring

The photocrosslinking process was also followed by quartz crystal microbalance with a dissipation monitoring device (QCM-D). Figure 4 reports the Δf and ΔD versus time plots. Event 1 and event 2 correspond to pouring of 400 µl of ptCS solution on the Au crystal and to UV irradiation of the ptCS solution, respectively. A high drop of frequency was recorded when the solution was placed on the sensor associated to the mass increased, at the same time the dissipation factor increased due to the low rigidity of the ptCS solutions.[47,48] The photocrosslinking process revealed a small reduction in the weight of the hydrogel (less than 10%) ascribed to water release during crosslinking (syneresis), while the rigidity of the hydrogel increased reducing the dissipation factor value.

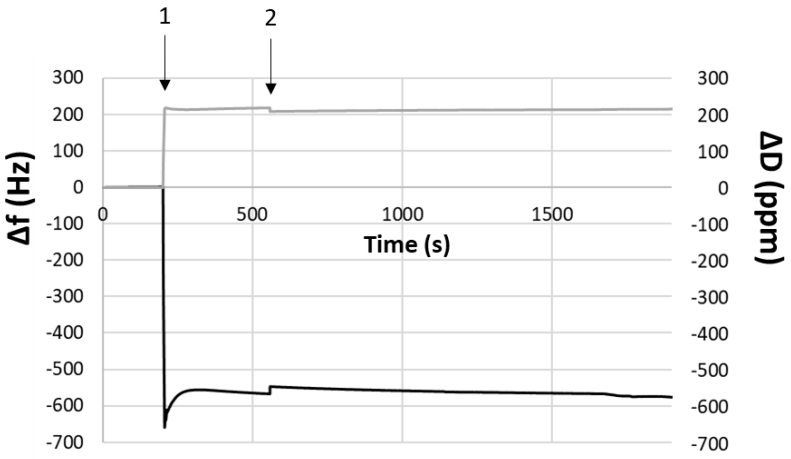

Figure 4. QCM-D plot of the third overtone of Δf and ΔD versus time. An Au sensor was coated with ptCS solution (event 1) and then the UV lamp was turned on to activate photocrosslinking (event 2).

Dissolution tests

The stability of the hydrogel in aqueous environment is a key feature to guarantee the formation of complex 3D cellularized structures. In the short period, the hydrogel should act as a support to allow for cell proliferation and maturation which, in the long term, should lead to the complete cell colonization of the 3D architecture while the hydrogel is dissolving.[49] The developed ptCS hydrogel showed fast dissolution characterized by weight loss in the first days and a less pronounced dissolution after 7 days (figure 5A) reaching a complete dissolution after 28 days. TGA analysis (figure 5B and C) revealed a compositional change of the ptCS hydrogel after 7 days in PBS ascribed to the release of the β-GP salt during the first steps of dissolution. Before the dissolution tests (ptCS hydrogel time 0 – figure 5 sample II), the TGA thermogram showed a first weight loss (around 20%) from 80°C to 100°C due to the presence of water. This strong water effect was mainly due to the hygroscopic behaviour of β-GP. Then, the degradation of CS occurred in the range from 230°C to 450°C as confirmed by the TGA thermogram of methacrylated CS powder (figure 5 sample I).[50] The weight loss during this step was around 30%. After 1 day in PBS; the TGA thermogram of the ptCS hydrogel (figure 5-sample III) did not show any significant differences compared to the ptCS

hydrogel at time 0. However, starting from 3 days in PBS the TGA thermogram of the ptCS hydrogel (figure 5, sample IV and V) illustrated a gradually decreasing weight loss due to the presence of water molecules linked to the β-GP. A curve trend similar to methacrylated CS powder was reached after 7 days in PBS. The stability of CS in physiological environment was confirmed by the slow dissolution rate after 7 days with no further changes detected by TGA. The TGA curve at 14 days (not shown) overlapped the TGA curve at 7 days.

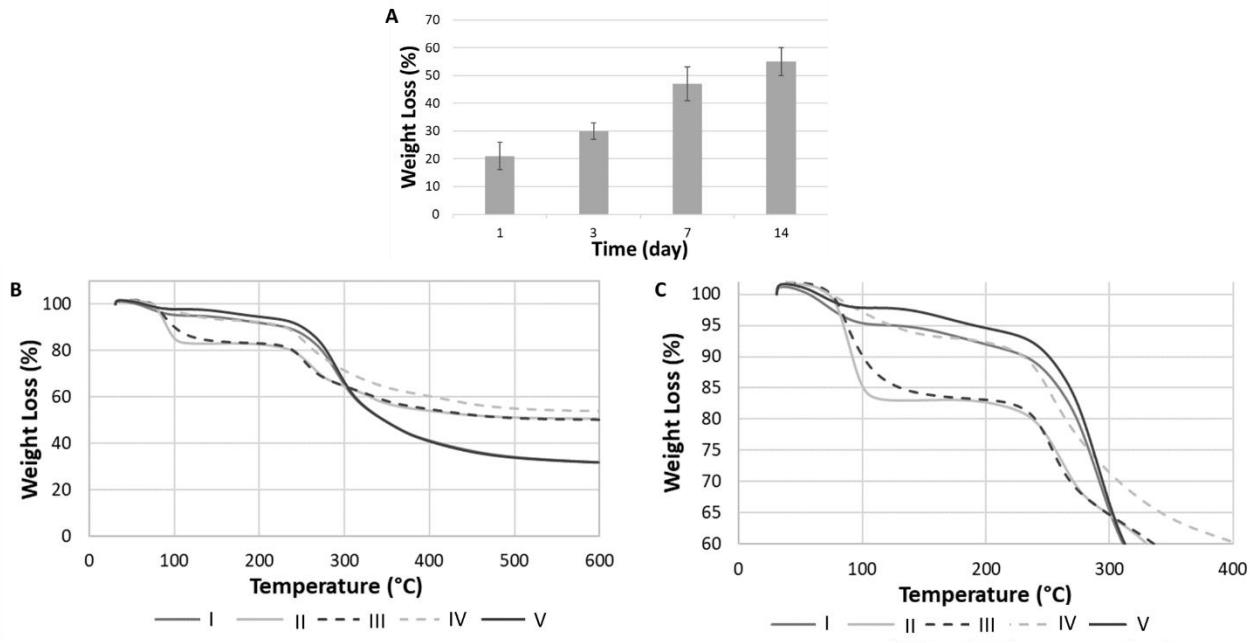

Figure 5.A) Weight loss of ptCS-hydrogels at different time points. **B)** representative curves of TGA analysis (temperature range from room temperature to 600°C) on ptCS hydrogels after dissolution tests and C) representative curves of TGA analysis (temperature range from room temperature to 400°C) on ptCS hydrogels after dissolution tests. Samples code: I) Methacrylated CS powder, II) ptCS hydrogel at time 0, III) ptCS hydrogel after 1 day, IV) ptCS hydrogel after 3 days, V) ptCS hydrogel after 7 days.

Assessment of ROS scavenging activity

CS is known for its antioxidant properties which are highly interesting in tissue regenration[51] as it can counteract detrimental effects of reactive oxygen species (ROS). CS can thus have many beneficial effects on cells such as promoting neurite development and alignment[52], enhancing vessel regeneration[53] and increasing stem cells homing after transplantation[54]. It was therefore of interest to evaluate the potential effect of methacrylation on the antioxidant properties. ptCS hydrogels and CS hydrogels showed a value of 18.8±1.8 and 20.0±3.4 in troxol equivalent, respectively. This shows that antioxidant capacity of CS was not significantly affected by the methacrylation process. The ability of reducing oxidative stress in cells is a crucial feature of hydrogels with encapsulated cells, as the encapsulated cells reveal an abnormal accumulation of ROS which could negatively affect cell activities[55].

CS-based solution as bioink for 3D bioprinting

PtCS solution was successfully extruded to continuous and homogeneous strands using a 25G tip. A four-layer grid was obtained (figure 6A) by a layer by layer process. After printing one layer, the printing process was stopped for one minute to permit photopolymerization. However, the stability of the strand after printing was guaranteed thanks to the rise in temperature from printhead (4°C) to printbed (37°C) exerting the thermosensitive behaviour of the ptCS solution.[56] 3D structures without defects were obtained with a strain size around 500 µm (figure 6 B and C) with a high reliability compared to the CAD designed structure. The adhesion among different layers was qualitatively observed by immersion of the multilayers structures in aqueous solution and no delamination was observed after one day confirming a good adhesion of the printed layers and the stability of the 3D printed constructs in physiological environments.

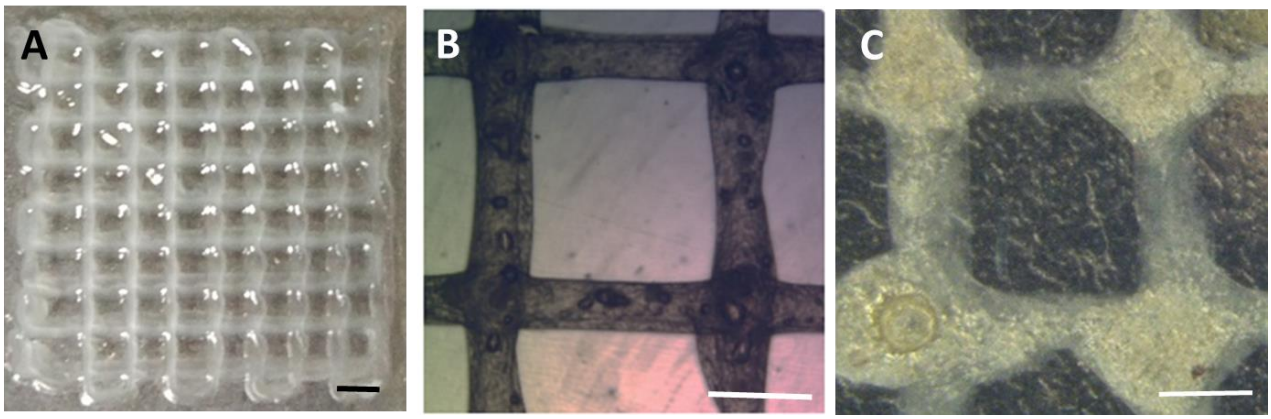

Figure 6. Representative images of 4-layer bioprinted grid immediately after printing (A,B) or after freeze-drying (C). Scale bars: 1 mm.

Cell viability assay: indirect tests

The biocompatibility of the developed hydrogel formulation was confirmed through indirect tests.[57] Three different cell lines were used to assess the applicability of this formulation in different biological environments. The viability of fibroblasts (NIH/3T3), osteoblast-like cells (Saos-2) and neuronal-like cells (SH-SY5Y) was not affected by ptCS hydrogels degradation products confirming the biocompatibility of the hydrogel (figure 7).

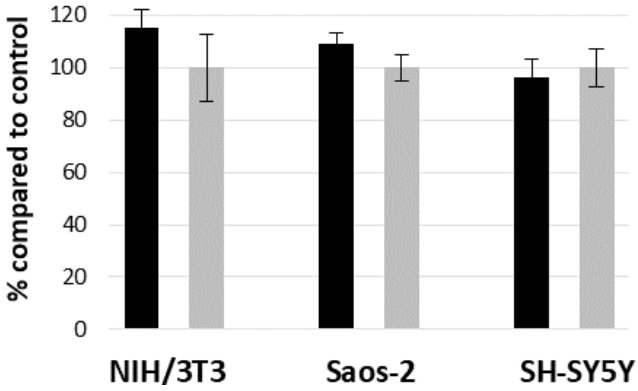

Figure 7. Cell viability of NIH/3T3, Saos-2, SH-SY5Y (black bars) compared to control conditions (grey bars).

Cell encapsulation and feasibility of cell loading bioprinting

Hydrogels represent the ideal candidate to house cells as their physico-chemical features allow mimicking of the key elements of the native extracellular matrix (ECM)[58] as they are highly swollen networks and they possess mechanical properties matching those of many soft tissues. Furthermore, the hydrogel composition can be easily tuned exposing biological functionality to the polymer backbone to provide a functional environment for cell adhesion and proliferation.[59] The novel pTCS hydrogel developed in this work combined mechanical properties in the range of few kPa similar to soft tissues[60,61] and a chemical composition which is expected to lead to excellent biological response[62]. The ability of this new formulation to encapsulate cells was proved by assessing the cell survival after encapsulation up to 7 days. NIH/3T3 were mixed into ptCS solution and then loaded into a 12 ml syringe to be placed into a 3D bioprinter. 100 µl drops or one-layer grips were printed using a 25G tips which have a size of 0.455 µm showing a good printing resolution without strongly affecting cell survival.[63] Immediately after printing, cells were well dispersed into the bioink and showed a rounded shape suggesting the adhesion process had not occurred yet (figure 8). However, after 24 hours cell shape revealed cell spreading (figure 9A, figure 10A) within the bioinks confirming the excellent biological properties of the developed CS-based hydrogel. On the other hand, at 48 hours cell proliferation was observed with a high increase of cells within both the printed drop and the printed grid (figure 9B, figure 10B). Furthermore, cell migration out of the hydrogels was observed confirming the high permeability of the bioink to cells as well as to nutrients and waste products. After 7 days, the whole printed structures were colonized by cells (figure 9C, figure 10C). Very few apoptotic cells (red dots in figure 9 C,D,E, figure 10 C,D,E) were observed at each time point highlighting the high biocompatibility of the developed hydrogel as well as of the processing technology. These results confirmed the ability of the developed ptCS solution to be processed through bioprinting into complex 3D structure as well as the potential to induce cell growth into the printed structure.

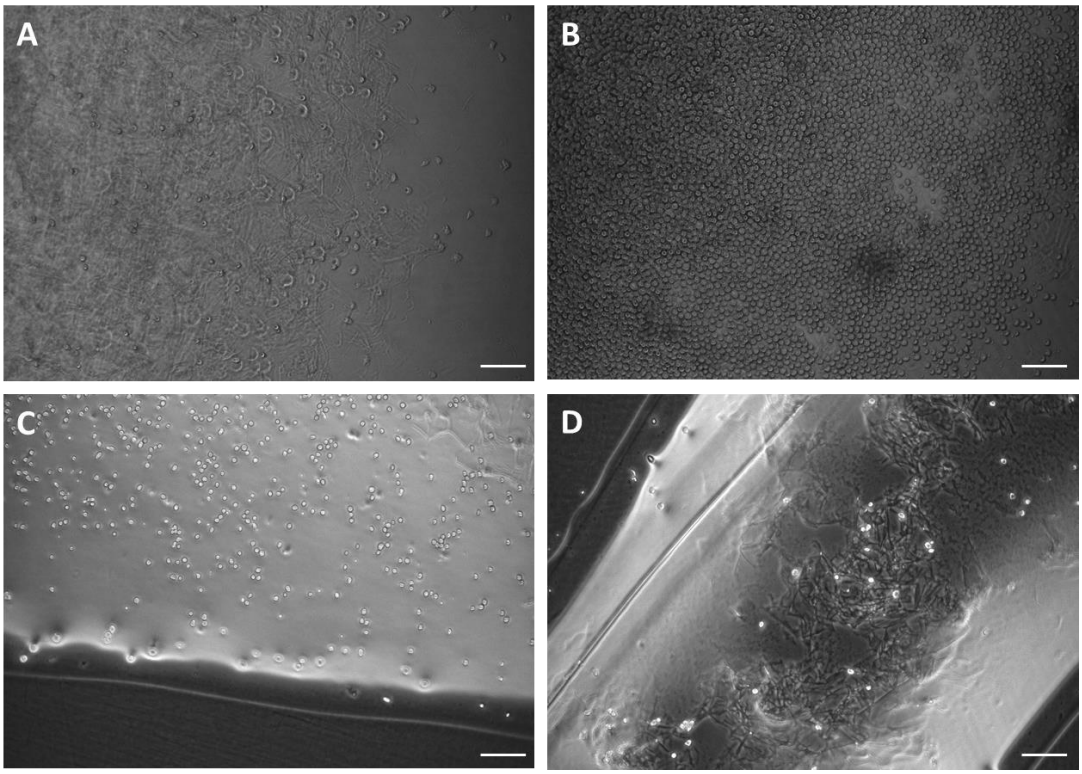

Figure 8. Light microscope images of NIH/3T3 cells encapsulated into drops (A, B) and lines (C, D) immediately after bioprinting. Scale bars 100 µm.

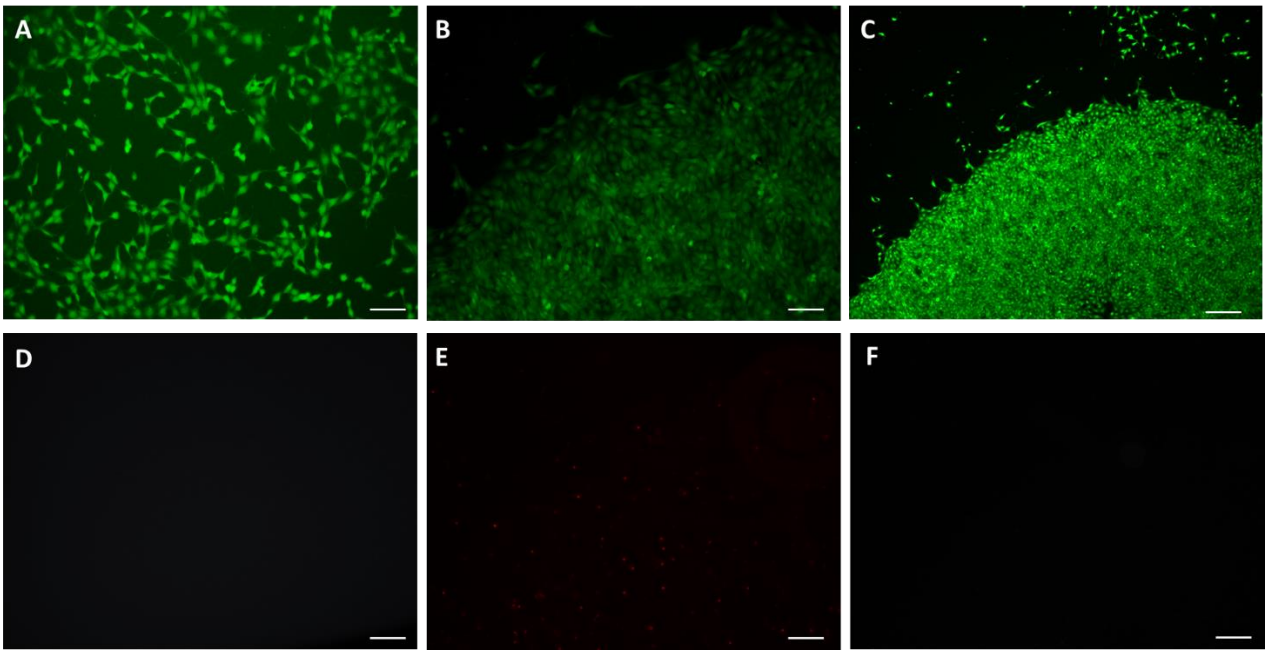

Figure 9. Live/dead assay of NIH/3T3 cells encapsulated into 100 µl-drop of ptCS hydrogels at 24h (A,D), 48h (B,E) and 120 h (C,F). Live cells are reported in green (A,B,C) while dead cells are in red (D,E, F). Scale bars: 100 µm (A,B,D,E) and 250 µm (C,F).

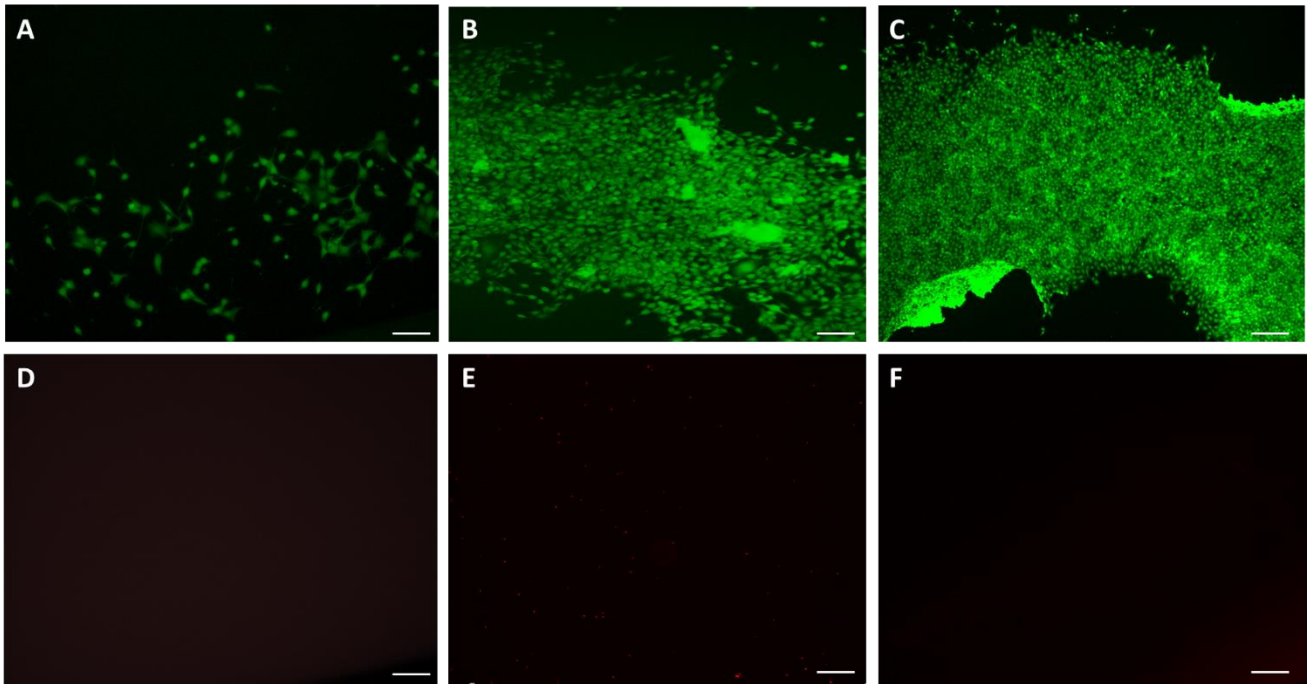

Figure 10. Live/dead assay of NIH/3T3 cells encapsulated into printed one-layer grid of ptCS hydrogels at 24 h (A,D), 48 h (B,E) and 120 h (C,F). Live cells are reported in green (A,B,C) while dead cells are in red (D,E, F). Scale bars: 100 µm (A,B,D,E) and 250 µm (C,F).

CONCLUSION

A photocurable chitosan formulation, fulfilling all the requirements for a successful bioink, was prepared. The designed composite CS bioink allowed bioprinting of high resolution structures thanks to the double crosslinking mechanism. It could be mixed with cells, it gelled upon temperature increase and UV irradiation (wavelength 365 nm) and it exhibited no cytotoxic effects on fibroblasts, osteoblast-like and neuronal-like cells. The developed bioink did not adversely affect the hosting cells and allowed cell proliferation and organization towards tissue formation. The cell-laden ability of the developed CS-based hydrogel and its' processability thought 3D bioprinting without causing cell damage was confirmed. Accurate 3D structures with good biocompatibility were successfully fabricated, giving promising prospects for the applicability of the developed bioink for recreation of complex living tissues.

Author Contributions

Chiara Tonda-Turo: Conceptualization, Methodology, Investigation, Supervision, Writing - Original Draft; **Irene Carmagnola**: Investigation, Writing - Original Draft; **Annalisa Chiappone**: Investigation, Writing - Original Draft; **Zhaoxuan Feng**: Investigation, Writing - Original Draft; **Gianluca Ciardelli**: Conceptualization, Writing - Review & Editing, Resources; **Minna Hakkarainen**: Conceptualization, Writing - Review & Editing, Resources; **Marco Sangermano**: Conceptualization, Writing - Review & Editing, Funding acquisition

Acknowledgment

The project “Biobased photocurable hydrogels” is sponsored by Politecnico di Torino, with the support of the Compagnia di San Paolo, Torino, within the framework of the “Call for Joint Projects for the internationalization of Research”.

ABBREVIATIONS

β-GP, β glycerol phosphate salt; CS chitosan; DMEM (Dulbecco's Modified Eagle Medium); EWC, Equilibrium Water Content; GelMa, gelatin methacrylate; LAP, lithium phenyl-2,4,6-trimethylbenzoylphosphinate; PEGDA, poly(ethylene glycol) diacrylate; ptCS, photo and thermo sensitive chitosan; QCM-D, Quartz crystal microbalance with dissipation monitoring device; ROS, reactive oxygen species; TERM, tissue engineering and regenerative medicine; WL, weight loss.

REFERENCES

[1] I.G. Lesci, L. Ciocca, N. Roveri, Biomimetic customized composite scaffolds and translational models for the bone regenerative medicine using CAD-CAM technology, in: Handb. Bioceram. Biocomposites, 2016. https://doi.org/10.1007/978-3-319-12460-5_28.

[2] S.A. Park, H.J. Lee, K.S. Kim, S.J. Lee, J.T. Lee, S.Y. Kim, N.H. Chang, S.Y. Park, In vivo evaluation of 3D-printed polycaprolactone scaffold implantation combined with β-TCP powder for alveolar bone augmentation in a beagle defect model, Materials (Basel). (2018). https://doi.org/10.3390/ma11020238.

[3] S. Derakhshanfar, R. Mbeleck, K. Xu, X. Zhang, W. Zhong, M. Xing, 3D bioprinting for biomedical devices and tissue engineering: A review of recent trends and advances, Bioact. Mater. (2018). https://doi.org/10.1016/j.bioactmat.2017.11.008.

[4] L.S. Neves, M.T. Rodrigues, R.L. Reis, M.E. Gomes, Current approaches and future

perspectives on strategies for the development of personalized tissue engineering therapies, Expert Rev. Precis. Med. Drug Dev. (2016). https://doi.org/10.1080/23808993.2016.1140004.

[5] K. Tappa, U. Jammalamadaka, Novel biomaterials used in medical 3D printing techniques, J. Funct. Biomater. (2018). https://doi.org/10.3390/jfb9010017.

[6] J. Jang, J.Y. Park, G. Gao, D.W. Cho, Biomaterials-based 3D cell printing for next-generation therapeutics and diagnostics, Biomaterials. (2018). https://doi.org/10.1016/j.biomaterials.2017.11.030.

[7] L. Ciocca, D. Donati, I.G. Lesci, B. Dozza, S. Duchi, O. Mezini, A. Spadari, N. Romagnoli, R. Scotti, N. Roveri, Custom-made novel biomimetic composite scaffolds for the bone regenerative medicine, Mater. Lett. (2014). https://doi.org/10.1016/j.matlet.2014.08.097.

[8] P. He, J. Zhao, J. Zhang, B. Li, Z. Gou, M. Gou, X. Li, Bioprinting of skin constructs for wound healing, Burn. Trauma. (2018). https://doi.org/10.1186/s41038-017-0104-x.

[9] A. Lee, A.R. Hudson, D.J. Shiwarski, J.W. Tashman, T.J. Hinton, S. Yerneni, J.M. Bliley, P.G. Campbell, A.W. Feinberg, 3D bioprinting of collagen to rebuild components of the human heart, Science (80-.). (2019). https://doi.org/10.1126/science.aav9051.

[10] N.Y.C. Lin, K.A. Homan, S.S. Robinson, D.B. Kolesky, N. Duarte, A. Moisan, J.A. Lewis, Renal reabsorption in 3D vascularized proximal tubule models, Proc. Natl. Acad. Sci. U. S. A. (2019). https://doi.org/10.1073/pnas.1815208116.

[11] J. Gopinathan, I. Noh, Recent trends in bioinks for 3D printing, Biomater. Res. (2018). https://doi.org/10.1186/s40824-018-0122-1.

[12] V.K. Lee, G. Dai, Printing of Three-Dimensional Tissue Analogs for Regenerative Medicine, Ann. Biomed. Eng. (2017). https://doi.org/10.1007/s10439-016-1613-7.

[13] S. Mehrotra, J.C. Moses, A. Bandyopadhyay, B.B. Mandal, 3D Printing/Bioprinting Based Tailoring of in Vitro Tissue Models: Recent Advances and Challenges, ACS Appl. Bio Mater. (2019). https://doi.org/10.1021/acsabm.9b00073.

[14] S.W. Kim, D.Y. Kim, H.H. Roh, H.S. Kim, J.W. Lee, K.Y. Lee, Three-Dimensional Bioprinting of Cell-Laden Constructs Using Polysaccharide-Based Self-Healing Hydrogels, Biomacromolecules. (2019). https://doi.org/10.1021/acs.biomac.8b01589.

[15] M. Boido, M. Ghibaudi, P. Gentile, E. Favaro, R. Fusaro, C. Tonda-Turo, Chitosan-based hydrogel to support the paracrine activity of mesenchymal stem cells in spinal cord injury treatment, Sci. Rep. (2019). https://doi.org/10.1038/s41598-019-42848-w.

[16] M. Boffito, P. Sirianni, A.M. Di Rienzo, V. Chiono, Thermosensitive block copolymer hydrogels based on poly(ε-caprolactone) and polyethylene glycol for biomedical applications: State of the art and future perspectives., J. Biomed. Mater. Res. A. (2014). https://doi.org/10.1002/jbm.a.35253.

[17] Y. Wu, Z.Y. (William) Lin, A.C. Wenger, K.C. Tam, X. (Shirley) Tang, 3D bioprinting of liver-mimetic construct with alginate/cellulose nanocrystal hybrid bioink, Bioprinting. (2018). https://doi.org/10.1016/j.bprint.2017.12.001.

[18] F.E. Freeman, D.J. Kelly, Tuning alginate bioink stiffness and composition for controlled growth factor delivery and to spatially direct MSC Fate within bioprinted tissues, Sci. Rep. (2017). https://doi.org/10.1038/s41598-017-17286-1.

[19] N. Ashammakhi, S. Ahadian, C. Xu, H. Montazerian, H. Ko, R. Nasiri, N. Barros, A. Khademhosseini, Bioinks and bioprinting technologies to make heterogeneous and biomimetic tissue constructs, Mater. Today Bio. (2019). https://doi.org/10.1016/j.mtbio.2019.100008.

[20] I. Donderwinkel, J.C.M. Van Hest, N.R. Cameron, Bio-inks for 3D bioprinting: Recent advances and future prospects, Polym. Chem. (2017). https://doi.org/10.1039/c7py00826k.

[21] M.T. Poldervaart, B. Goversen, M. De Ruijter, A. Abbadessa, F.P.W. Melchels, F.C. Öner, W.J.A. Dhert, T. Vermonden, J. Alblas, 3D bioprinting of methacrylated hyaluronic acid (MeHA) hydrogel with intrinsic osteogenicity, PLoS One. (2017). https://doi.org/10.1371/journal.pone.0177628.

[22] H.W. Ooi, C. Mota, A. Tessa Ten Cate, A. Calore, L. Moroni, M.B. Baker, Thiol-Ene Alginate Hydrogels as Versatile Bioinks for Bioprinting, Biomacromolecules. (2018). https://doi.org/10.1021/acs.biomac.8b00696.

[23] K. Yue, G. Trujillo-de Santiago, M.M. Alvarez, A. Tamayol, N. Annabi, A. Khademhosseini, Synthesis, properties, and biomedical applications of gelatin methacryloyl (GelMA) hydrogels, Biomaterials. (2015). https://doi.org/10.1016/j.biomaterials.2015.08.045.

[24] J. Yin, M. Yan, Y. Wang, J. Fu, H. Suo, 3D Bioprinting of Low-Concentration Cell-Laden Gelatin Methacrylate (GelMA) Bioinks with a Two-Step Cross-linking Strategy, ACS Appl. Mater. Interfaces. (2018). https://doi.org/10.1021/acsami.7b16059.

[25] I. Pepelanova, K. Kruppa, T. Scheper, A. Lavrentieva, Gelatin-methacryloyl (GelMA) hydrogels with defined degree of functionalization as a versatile toolkit for 3D cell culture and extrusion bioprinting, Bioengineering. (2018). https://doi.org/10.3390/bioengineering5030055.

[26] W. Zhu, H. Cui, B. Boualam, F. Masood, E. Flynn, R.D. Rao, Z.Y. Zhang, L.G. Zhang, 3D bioprinting mesenchymal stem cell-laden construct with core-shell nanospheres for cartilage tissue engineering, Nanotechnology. (2018). https://doi.org/10.1088/1361-6528/aaafa1.

[27] J.D. Schneible, A. Singhal, R.L. Lilova, C.K. Hall, A. Grafmüller, S. Menegatti, Tailoring the Chemical Modification of Chitosan Hydrogels to Fine-Tune the Release of a Synergistic Combination of Chemotherapeutics, Biomacromolecules. (2019). https://doi.org/10.1021/acs.biomac.9b00707.

[28] N.P. Birch, L.E. Barney, E. Pandres, S.R. Peyton, J.D. Schiffman, Thermal-responsive behavior of a cell compatible chitosan/pectin hydrogel, Biomacromolecules. (2015). https://doi.org/10.1021/acs.biomac.5b00425.

[29] M. Sahranavard, A. Zamanian, F. Ghorbani, M.H. Shahrezaee, A critical review on three dimensional-printed chitosan hydrogels for development of tissue engineering, Bioprinting. (2020). https://doi.org/10.1016/j.bprint.2019.e00063.

[30] X. Zhang, D. Yang, J. Nie, Chitosan/polyethylene glycol diacrylate films as potential wound dressing material, Int. J. Biol. Macromol. (2008). https://doi.org/10.1016/j.ijbiomac.2008.08.010.

[31] E.A. Grebenik, A.M. Surin, K. Bardakova, T. Demina, N. Minaev, N. Veryasova, M. Artyukhova, I. Krasilnikova, Z.V. Bakaeva, E.G. Sorokina, D. Boiarkin, T. Akopova, V. Pinelis, P.S. Timashev, Chitosan-g-oligo(L,L-lactide) copolymer hydrogel for nervous tissue regeneration in glutamate excitotoxicity: *In vitro* feasibility evaluation, Biomed. Mater. (2019). https://doi.org/10.1088/1748-605x/ab6228.

[32] Z. Feng, M. Hakkarainen, H. Grützmacher, A. Chiappone, M. Sangermano, Photocrosslinked Chitosan Hydrogels Reinforced with Chitosan-Derived Nano-Graphene Oxide, Macromol. Chem. Phys. (2019). https://doi.org/10.1002/macp.201900174.

[33] L. Zhu, K.M. Bratlie, pH sensitive methacrylated chitosan hydrogels with tunable physical and chemical properties, Biochem. Eng. J. (2018). https://doi.org/10.1016/j.bej.2017.12.012.

[34] M. Diolosà, I. Donati, G. Turco, M. Cadenaro, R. Di Lenarda, L. Breschi, S. Paoletti, Use of methacrylate-modified chitosan to increase the durability of dentine bonding systems, Biomacromolecules. (2014). https://doi.org/10.1021/bm5014124.

[35] O.M. Kolawole, W.M. Lau, V. V. Khutoryanskiy, Methacrylated chitosan as a polymer with enhanced mucoadhesive properties for transmucosal drug delivery, Int. J. Pharm. (2018). https://doi.org/10.1016/j.ijpharm.2018.08.034.

[36] Y. Zhou, K. Liang, C. Zhang, J. Li, H. Yang, X. Liu, X. Yin, D. Chen, W. Xu, P. Xiao, Photocrosslinked methacrylated chitosan-based nanofibrous scaffolds as potential skin substitute, Cellulose. (2017). https://doi.org/10.1007/s10570-017-1433-4.

[37] S. Kim, Z.K. Cui, J. Fan, A. Fartash, T.L. Aghaloo, M. Lee, Photocrosslinkable chitosan hydrogels functionalized with the RGD peptide and phosphoserine to enhance osteogenesis, J. Mater. Chem. B. (2016). https://doi.org/10.1039/c6tb01154c.

[38] M. Boido, R. Rupa, D. Garbossa, M. Fontanella, A. Ducati, A. Vercelli, Embryonic and adult stem cells promote raphespinal axon outgrowth and improve functional outcome following spinal hemisection in mice., Eur. J. Neurosci. (2009). https://doi.org/10.1111/j.1460-9568.2009.06879.x.

[39] C. Pontremoli, M. Boffito, S. Fiorilli, R. Laurano, A. Torchio, A. Bari, C. Tonda-Turo, G. Ciardelli, C. Vitale-Brovarone, Hybrid injectable platforms for the in situ delivery of therapeutic ions from mesoporous glasses, Chem. Eng. J. (2018). https://doi.org/10.1016/j.cej.2018.01.073.

[40] S. Supper, N. Anton, N. Seidel, M. Riemenschnitter, C. Curdy, T. Vandamme, Thermosensitive chitosan/glycerophosphate-based hydrogel and its derivatives in pharmaceutical and biomedical applications, Expert Opin. Drug Deliv. (2014). https://doi.org/10.1517/17425247.2014.867326.

[41] S. Supper, N. Anton, N. Seidel, M. Riemenschnitter, C. Schoch, T. Vandamme, Rheological study of chitosan/polyol-phosphate systems: Influence of the polyol part on the thermo-induced gelation mechanism, Langmuir. (2013). https://doi.org/10.1021/la401993q.

[42] C. Tonda-Turo, F. Ruini, M. Ramella, F. Boccafoschi, P. Gentile, E. Gioffredi, G. Falvo D'Urso Labate, G. Ciardelli, Non-covalently crosslinked chitosan nanofibrous mats prepared by electrospinning as substrates for soft tissue regeneration, Carbohydr. Polym. 162 (2017). https://doi.org/10.1016/j.carbpol.2017.01.050.

[43] K. Maji, S. Dasgupta, K. Pramanik, A. Bissoyi, Preparation and characterization of gelatin-chitosan-nanoβ-TCP based scaffold for orthopaedic application, Mater. Sci. Eng. C. (2018). https://doi.org/10.1016/j.msec.2018.02.001.

[44] E. Fantino, I. Roppolo, D. Zhang, J. Xiao, A. Chiappone, M. Castellino, Q. Guo, C.F. Pirri, J. Yang, 3D Printing/Interfacial Polymerization Coupling for the Fabrication of Conductive Hydrogel, Macromol. Mater. Eng. (2018). https://doi.org/10.1002/mame.201700356.

[45] J. Wang, A. Chiappone, I. Roppolo, F. Shao, E. Fantino, M. Lorusso, D. Rentsch, K.

Dietliker, C.F. Pirri, H. Grützmacher, All-in-One Cellulose Nanocrystals for 3D Printing of Nanocomposite Hydrogels, Angew. Chemie - Int. Ed. (2018). https://doi.org/10.1002/anie.201710951.

[46] C.D. O'Connell, B. Zhang, C. Onofrillo, S. Duchi, R. Blanchard, A. Quigley, J. Bourke, S. Gambhir, R. Kapsa, C. Di Bella, P. Choong, G.G. Wallace, Tailoring the mechanical properties of gelatin methacryloyl hydrogels through manipulation of the photocrosslinking conditions, Soft Matter. (2018). https://doi.org/10.1039/c7sm02187a.

[47] P. Åsberg, P. Björk, F. Höök, O. Inganäs, Hydrogels from a water-soluble Zwitterionic polythiophene: Dynamics under pH change and biomolecular interactions observed using quartz crystal microbalance With dissipation monitoring, Langmuir. (2005). https://doi.org/10.1021/la050479e.

[48] C. Tonda-Turo, I. Carmagnola, G. Ciardelli, Quartz Crystal Microbalance With Dissipation Monitoring: A Powerful Method to Predict the in vivo Behavior of Bioengineered Surfaces, Front. Bioeng. Biotechnol. (2018). https://doi.org/10.3389/fbioe.2018.00158.

[49] G.D. Nicodemus, S.J. Bryant, Cell encapsulation in biodegradable hydrogels for tissue engineering applications, Tissue Eng. - Part B Rev. (2008). https://doi.org/10.1089/ten.teb.2007.0332.

[50] S. Kumar, J. Koh, Physiochemical, optical and biological activity of chitosan-chromone derivative for biomedical applications, Int. J. Mol. Sci. (2012). https://doi.org/10.3390/ijms13056102.

[51] M.T. Yen, J.H. Yang, J.L. Mau, Antioxidant properties of chitosan from crab shells, Carbohydr. Polym. (2008). https://doi.org/10.1016/j.carbpol.2008.05.003.

[52] A. Marino, C. Tonda-Turo, D. De Pasquale, F. Ruini, G. Genchi, S. Nitti, V. Cappello, M. Gemmi, V. Mattoli, G. Ciardelli, G. Ciofani, Gelatin/nanoceria nanocomposite fibers as antioxidant scaffolds for neuronal regeneration, Biochim. Biophys. Acta - Gen. Subj. 1861 (2017). https://doi.org/10.1016/j.bbagen.2016.11.022.

[53] S. Shafi, H.R. Ansari, W. Bahitham, S. Aouabdi, The Impact of Natural Antioxidants on the Regenerative Potential of Vascular Cells, Front. Cardiovasc. Med. (2019). https://doi.org/10.3389/fcvm.2019.00028.

[54] W. Zeng, J. Xiao, G. Zheng, F. Xing, G.L. Tipoe, X. Wang, C. He, Z.Y. Chen, Y. Liu, Antioxidant treatment enhances human mesenchymal stem cell anti-stress ability and therapeutic efficacy in an acute liver failure model, Sci. Rep. (2015). https://doi.org/10.1038/srep11100.

[55] Y. Martín-Martín, L. Fernández-García, M.H. Sanchez-Rebato, N. Marí-Buyé, F.J. Rojo, J. Pérez-Rigueiro, M. Ramos, G. V. Guinea, F. Panetsos, D. González-Nieto, Evaluation of Neurosecretome from Mesenchymal Stem Cells Encapsulated in Silk Fibroin Hydrogels, Sci. Rep. (2019). https://doi.org/10.1038/s41598-019-45238-4.

[56] R. Suntornnond, J. An, C.K. Chua, Bioprinting of Thermoresponsive Hydrogels for Next Generation Tissue Engineering: A Review, Macromol. Mater. Eng. (2017). https://doi.org/10.1002/mame.201600266.

[57] M. Boffito, E. Gioffredi, V. Chiono, S. Calzone, E. Ranzato, S. Martinotti, G. Ciardelli, Novel polyurethane-based thermosensitive hydrogels as drug release and tissue engineering platforms: Design and in vitro characterization, Polym. Int. (2016). https://doi.org/10.1002/pi.5080.

[58] S.R. Caliari, J.A. Burdick, A practical guide to hydrogels for cell culture, Nat. Methods. (2016). https://doi.org/10.1038/nmeth.3839.

[59] V. Pérez-Luna, O. González-Reynoso, Encapsulation of Biological Agents in Hydrogels for Therapeutic Applications, Gels. (2018). https://doi.org/10.3390/gels4030061.

[60] N. Fekete, A. V. Béland, K. Campbell, S.L. Clark, C.A. Hoesli, Bags versus flasks: a comparison of cell culture systems for the production of dendritic cell–based immunotherapies, Transfusion. (2018). https://doi.org/10.1111/trf.14621.

[61] P.M. Gilbert, K.L. Havenstrite, K.E.G. Magnusson, A. Sacco, N.A. Leonardi, P. Kraft, N.K. Nguyen, S. Thrun, M.P. Lutolf, H.M. Blau, Substrate elasticity regulates skeletal muscle stem cell self-renewal in culture, Science (80-.). (2010). https://doi.org/10.1126/science.1191035.

[62] R.C.F. Cheung, T.B. Ng, J.H. Wong, W.Y. Chan, Chitosan: An update on potential biomedical and pharmaceutical applications, Mar. Drugs. (2015). https://doi.org/10.3390/md13085156.

[63] G. Cidonio, M. Glinka, J.I. Dawson, R.O.C. Oreffo, The cell in the ink: Improving biofabrication by printing stem cells for skeletal regenerative medicine, Biomaterials. (2019). https://doi.org/10.1016/j.biomaterials.2019.04.009.

Table of Contents graphic (TOC)

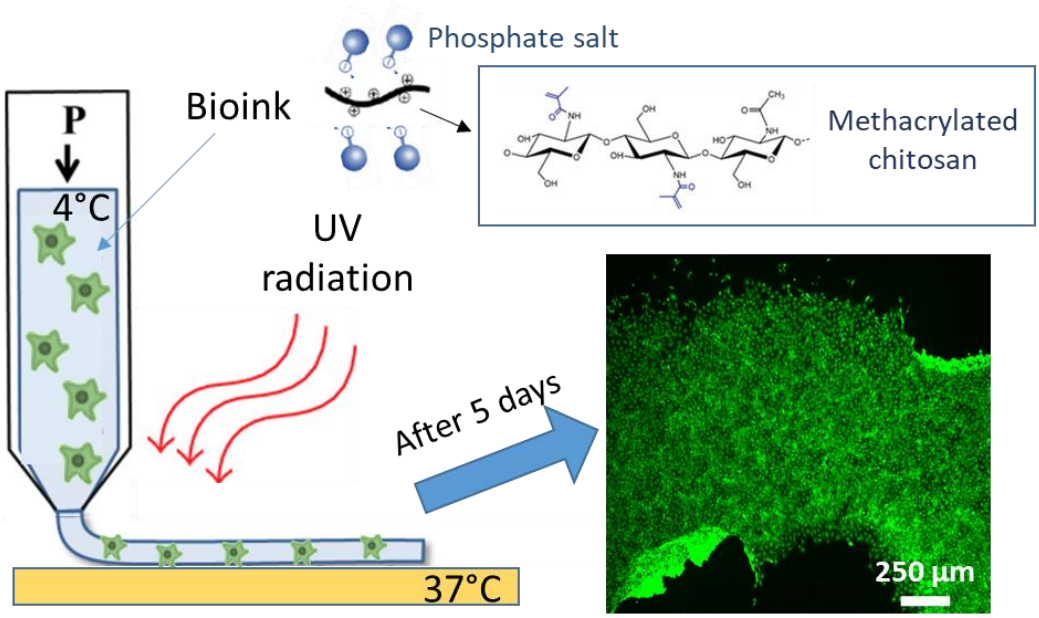
Phosphate salt
Bioink
Methacrylated chitosan
P
4°C
UV radiation
After 5 days
37°C
250 µm